Ecotoxicology and Environmental Safety 230 (2022) 113126

Contents lists available at ScienceDirect

Ecotoxicology and Environmental Safety

journal homepage: www.elsevier.com/locate/ecoenv

Accelerated toluene degradation over forests around megacities in southern China

Qinqin Li [a], Daocheng Gong [a,b,c], Yu Wang [a,b,c], Hao Wang [a,b,c,*], Wenlu Wang [a,b,c], Gengchen Wu [a,b], Hai Guo [b,d], Boguang Wang [a,b,c,*]

[a] Institute for Environmental and Climate Research, Jinan University, Guangzhou, China
[b] Australia-China Centre for Air Quality Science and Management (Guangdong), Guangzhou 511443, China
[c] Guangdong-Hongkong-Macau Joint Laboratory of Collaborative Innovation for Environmental Quality, Guangzhou, China
[d] Air Quality Studies, Department of Civil and Environmental Engineering, The Hong Kong Polytechnic University, Hong Kong, China

ARTICLE INFO

Edited by Dr G Liu

Keywords:
Toluene
Nanling Mountains
Pearl River Delta
Degradation rate
Atmospheric oxidative capacity

ABSTRACT

Toluene is a typical anthropogenic pollutant that has profound impacts on air quality, climate change, and human health, but its sources and sinks over forests surrounding megacities remain unclear. The Nanling Mountains (NM) is a large subtropical forest and is adjacent to the Pearl River Delta (PRD) region, a well-known hotspot for toluene emissions in southern China. However, unexpectedly low toluene concentrations (0.16 ± 0.20 ppbv) were observed at a mountaintop site in NM during a typical photochemical period. A backward trajectory analysis categorized air masses received at the site into three groups, namely, air masses from the PRD, those from central China, and from clean areas. The results revealed more abundant toluene and its key oxidation products, for example, benzaldehyde in air masses mixed with urban plumes from the PRD. Furthermore, a more than three times faster degradation rate of toluene was found in this category of air masses, indicating more photochemical consumption in NM under PRD outflow disturbance. Compared to the categorized clean and central China plumes, the simulated OH peak level in the PRD plumes (15.8 ± 2.2 × 10^6 molecule cm^{-3}) increased by approximately 30% and 55%, respectively, and was significantly higher than the reported values at other background sites worldwide. The degradation of toluene in the PRD plumes was most likely accelerated by increased atmospheric oxidative capacity, which was supported by isoprene ozonolysis reactions. Our results indicate that receptor forests around megacities are not only highly polluted by urban plumes, but also play key roles in environmental safety by accelerating the degradation rate of anthropogenic pollutants.

1. Introduction

Toluene plays a vital role in air pollution and climate change, acting as one of the most key precursors of ozone (O_3) and secondary organic aerosols (SOA) (Wu et al., 2017). Toluene emissions are dominated by various anthropogenic activities, such as solvent usage, industrial processes and vehicular exhaust (Song et al., 2007). In addition, toluene is sufficiently long-lived to be transported globally over long distances (Okamoto and Tanimoto, 2016). Increased human activities have resulted in toluene being measured at most remote sites around the world (Paralovo et al., 2019). As well as its toxic characteristics for humans and other organisms (Xu et al., 2020), the negative impact of toluene on a regional and global scale is of increasing concern (Yan et al., 2019).

Toluene degradation mainly occurs through reactions with hydroxyl (OH) radicals (Cabrera-Perez et al., 2016), and benzaldehyde is a typical ring-retaining product in toluene-OH photochemistry (Atkinson and Arey, 2003). According to Cabrera-Perez et al. (2016), considering that the global spatial pattern is dominated by chemical formation and resembles toluene distributions, the variation in benzaldehyde should be a suitable parameter related to toluene degradation. However, a dramatic drop in toluene concentration over forested areas has been reported (Custódio et al., 2010; Martin et al., 2017). Unexpectedly high OH levels in forest atmospheres with abundant biogenic volatile organic compounds (BVOCs) and low nitrogen oxide (NO_x) have been of particular concern (Liu et al., 2018), and are suggested to be regenerated by the reaction of BVOC-derived RO_2 radicals and HO_2 (Khan et al., 2021). Recent chamber studies have revealed an enhanced consumption of

* Corresponding authors at: Institute for Environmental and Climate Research, Jinan University, Guangzhou, China.
E-mail addresses: wanghao@jnu.edu.cn (H. Wang), tbongue@jnu.edu.cn (B. Wang).

https://doi.org/10.1016/j.ecoenv.2021.113126
Received 4 August 2021; Received in revised form 23 December 2021; Accepted 24 December 2021
Available online 30 December 2021

toluene under complex oxidation scenarios involving BVOCs with promoted photochemical reactions (Chen et al., 2017). Therefore, a hypothesis that forests act as significant sink pools for anthropogenic toluene is reasonable, and that studies on toluene degradation in forested areas are essential to better understanding the significant effects of toluene on regional air quality. However, toluene degradation in forests remain less studied than that in urban conditions.

The Pearl River Delta (PRD) region in southern China is a well-known toluene hotspot (Mo et al., 2018), with rapidly increasing emissions (Fang et al., 2016). Simultaneously, significantly high OH concentrations have revealed more active photochemistry in this region (Lu et al., 2018). With worsening photochemical pollution and elevating O_3 pollution, abundant toluene degradation over southern China is a cause for concern. The Nanling Mountains (NM) comprise large subtropical forests (200 km × 400 km) that are located to the north of the PRD region (Lin et al., 2019), and particularly strong oxidative capacity has been reported here (Gong et al., 2018). Elevated glyoxal and methylglyoxal levels, which are two typical products of toluene oxidation, were observed in the NM in the presence of PRD plumes (Lv et al., 2019). Toluene levels in NM (Gong et al., 2018) were significantly lower than those at Mt. Tai (Ting et al., 2009) and Mt. Gongga (Zhang et al., 2014), which are regional receptor sites for the heavily polluted North China Plain and southwest China, respectively. Therefore, the significantly lower toluene in NM and the impact of PRD plumes require further investigation.

In this study, field measurements of toluene and benzaldehyde were conducted in NM during a photochemically polluted season in southern China, when air masses from the north, south, and east could be observed. Toluene degradation over NM, with and without urban air masses, was well characterized. This study aimed to elucidate (1) the concentration levels and temporal variations of toluene and its key oxidation products, (2) the quantitative assessment of the toluene degradation rate, and (3) the possible influence of urban outflows on the atmospheric oxidative capacity (AOC) over downwind forests. Our results further the understanding of toluene transformations in forests around megacities and provide more insights into mitigating aggravating regional photochemical pollution in southern China.

2. Experiment and methodology

2.1. Site description

Previous studies have demonstrated that toluene concentrations and atmospheric oxidative capacity in the regions surrounding NM are generally higher in autumn, which is the typical photochemical pollution season (Li and Wang, 2012; Zeng et al., 2019). Therefore, an intensive measurement campaign was conducted at the summit of NM (24.7°N, 112.9°E, 1690 m a.s.l.) from October 16 to November 5, 2016. The sampling site (Fig. 1) is located approximately 200 km from the center of the PRD region and is close to the border of Hunan Province in central China. It is located at the center of the Guangdong Nanling National Natural Reserve, surrounded by subtropical forests, and far from sources of anthropogenic emissions. During the sampling period, the sampling site was predominantly affected by easterly, southerly, and northerly air masses. NM receives polluted plumes from both the PRD region and central China under southerly and northerly winds, respectively, and the corresponding regional environmental effects require particular investigation. A detailed description of the site has been presented in a previous study by the present authors (Gong et al., 2018).

2.2. Measurement techniques

All instruments were housed in a laboratory where the room temperature was maintained at approximately 25 °C for 24 h to ensure instrument stability. The sampling system, measurement instruments, and calibration procedures were the same as those used in previous studies

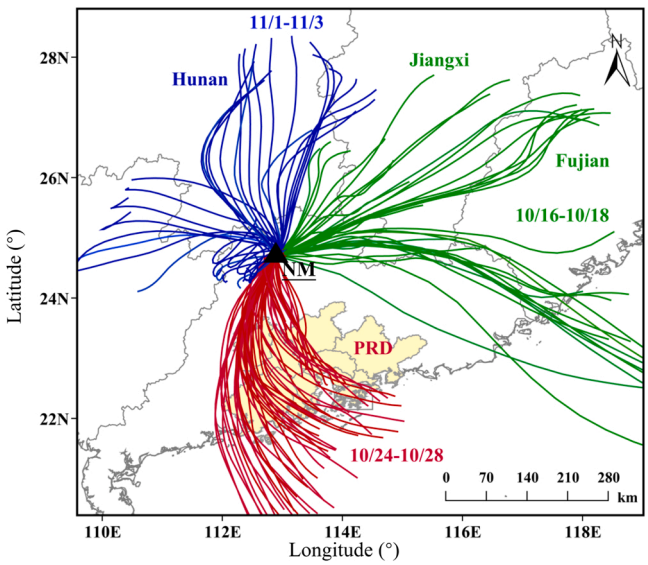

Fig. 1. Location of the Nanling Mountains (NM). The red, green and blue lines indicate the 24 h back-trajectory clusters arriving at the sampling site. The yellow shade indicates the PRD region. (For interpretation of the references to colour in this figure legend, the reader is referred to the web version of this article.)

by Gong et al. (2018) and Lv et al. (2019), brief summaries are presented here.

Trace gases (O_3, NO, NO_2, CO and SO_2 in this study) were monitored in real time using commercial instruments with a time resolution of 5 min. The detection limits for those trace gases were 0.5, 0.05, 0.05, 40 and 0.05 ppbv, respectively. The calibration of instruments was conducted weekly, and the examination of zero and span was performed every alternate day. According to Xu et al. (2013), NO_2 measured in this study was regarded as NO_2 * , which includes some oxidized reactive nitrogen. Meteorological parameters were also detected every 5 min, including temperature (Temp.), relative humidity (RH), wind speed, and wind direction.

Real-time toluene and benzene were analyzed by online gas chromatography-mass spectrometry (7820 A GC, 5977E MSD, Agilent Technologies Inc., USA) equipped with a cryogen-free trap preconcentration device (TH-PKU 300 B, Wuhan Tianhong Instrument Co. Ltd., China). The time resolution was set to 1 h. Before entering the system, particulate matter, moisture, and CO_2 were removed using a Teflon filter (0.25 μm pore size, 47 mm OD, MilliporeSigma, USA), a water management trap, and a soda asbestos tube, respectively. The flow rate was 60 mL min^{-1} and the sampling time was 5 min. The R^2 values for the calibration curves of toluene, benzene, and isoprene were higher than 0.99, and the precision was lower than 2%. The detection limits for toluene, benzene and isoprene were 0.002, 0.003 and 0.004 ppbv, respectively.

Benzaldehyde was simultaneously sampled into pentafluorophenyl hydrazine cartridges at a flow rate of 100 mL min^{-1} for 3 h (05:00–08:00, 09:00–12:00, 12:00–15:00, 15:00–18:00, 18:00–21:00, and 22:00–01:00 LT). O_3 was removed by coating saturated potassium iodide in a 1 m long helical copper tube before each sampling tube. All benzaldehyde samples were analyzed using an offline GC-MS system (7820 A GC/5977E MSD, Agilent Technologies Inc., USA). The R^2 value for the calibration of benzaldehyde was greater than 0.99. The detection limit for benzaldehyde is 0.005 ppbv. A total of 89 field samples have been collected during the campaign.

2.3. Calculation of photochemical degradation rate of toluene

OH radicals are the most important drivers of the photochemical

degradation of toluene and benzene in the atmosphere. The variation of toluene and benzene ratios (T/B) is widely used to reflect the characteristics of OH radicals, because the OH reaction rate of toluene is higher, while that of benzene is lower (Eq. (1)) (de Gouw et al., 2008). In addition, the principal mechanism for the decrease in the T/B ratios in the background atmosphere depends on oxidation with OH radicals (Martin et al., 2017). To quantitatively describe the degradation rate of toluene relating to benzene, Eq. (1) was converted to Eq. (2) as follows:

$$[OH] = \frac{Ln\left(\frac{T}{B}\right)_0 - Ln\left(\frac{T}{B}\right)_t}{\Delta t \times (k_T - k_B)} \quad (1)$$

$$\frac{\Delta Ln\left(\frac{T}{B}\right)}{\Delta t} = (k_T - k_B) \times [OH] \quad (2)$$

where T and B are the observed concentrations of toluene and benzene, respectively, and k_T and k_B represent the rate coefficients for toluene and benzene reactions with OH radicals (Atkinson and Arey, 2003), respectively. As presented in Eq. (2), the change in Ln(T/B) at a time interval of Δt, as ΔLn(T/B)/Δt, shows a linear relationship with OH radicals. Therefore, ΔLn(T/B)/Δt is a good parameter for evaluating the degradation rate of toluene in background areas. Notably, the contributions of physical processes, such as dilution and deposition, to ΔLn (T/B)/Δt were not considered in Eq. (2).

2.4. In situ OH radicals simulated by a chemical box model

The Master Chemical Mechanism (MCM version 3.2) (http: //mcm.leeds.ac.uk/MCM/) contains approximately 16,500 reactions involving 5900 chemical species (Saunders et al., 2003) and has been widely utilized to estimate the budgets of atmospheric oxidant radicals (Guo et al., 2013). This study applied the chemical box model to investigate the atmospheric oxidative capacity in NM, with measured meteorological parameters, trace gases (O_3, NO, NO_2, CO and SO_2 in this study), and VOC species as input. HONO, as one of the key sources of OH radicals (Zhou et al., 2001), was not measured in this study. A sensitivity analysis corresponding to the variations in NO_2 and HONO in NM has shown that the daytime OH concentrations simulated by MCM were overestimated by approximately 20% (Gong et al., 2018). More detailed descriptions of the MCM are presented by Saunders et al. (2003) and Wang et al. (2018).

3. Results and discussion

3.1. Faster degradation of toluene in NM

The time series of hourly averaged levels of meteorological parameters and trace gases in NM are illustrated in Fig. S1. Toluene concentrations varied significantly throughout the sampling period. The average mixing ratio of toluene was 0.16 ± 0.20 ppbv, and the maximum value reached 1.60 ppbv. Table 1 presents the toluene concentrations observed at NM and those reported at other background sites worldwide. Compared to other background sites, the overall observations at regional background sites in China showed significantly higher toluene levels, particularly those sites distributed in southern China. This indicates that the massive toluene emissions in Chinese megacity clusters, particularly in the PRD region, have exerted extreme influences on regional atmospheric chemical conditions. For example, the highest background value of toluene was found on Mt. Dinghu, which is located in the PRD region.

However, it is clear that the toluene concentrations in NM were

Table 1
Average concentrations (ppbv) of toluene at the Nanling Mountains and other background sites worldwide (SD: standard deviation).

Site	Latitude, Longitude	Altitude (m a.s.l.)	Sampling period	Mean ± SD	Reference
Mt. Dinghu, China	23.17°N, 112.52°E	1000	Jan. 2005-Dec. 2008	2.27 ± 0.89	Wu et al. (2016a)
Mt. Tai Mo Shan, China	22.41°N, 114.12°E	640	Nov. 2010	1.58 ± 1.25	Fang et al. (2016)
Mt. Mang, China	40.26°N, 116.28°E	630	Sep.-Oct. 2007	1.32 ± 1.15	Suthawaree et al. (2012)
Mt. Lushan, China	29.58°N, 115.98°E	1165	Aug.-Sep. 2011	0.87	Yang et al. (2016)
Hok Tsui, China	22.22°N, 114.25°E	60	Oct.-Nov. 2015	0.48 ± 0.58	Data from HKPU*
Mt. Tai, China	36.25°N, 117.1°E	1534	Jun. 2006	0.47 ± 0.28	Ting et al. (2009)
Mt. Gongga, China	29.55°N, 102°E	1640	Jan. 2008-Dec. 2011	0.44 ± 0.33	Zhang et al. (2014)
Jinyunshan, China	30.38°N, 106.6°E	900	Aug.-Sep. 2015	0.40 ± 0.20	Li et al. (2018)
Mt. Wuyi, China	27.35°N, 117.43°E	1139	Dec.2016	0.33 ± 0.11	Hong et al. (2019)
Shangdianzi, China	40.65°N, 117.12°E	293.9	Sep.- Dec.2017	0.31 ± 0.34	Han et al. (2020)
Mt. Changbai, China	42.4°N, 128.47°E	763	Nov. 2011-Dec.2012	0.28 ± 0.29	Wu et al. (2016b)
Shennongjia, China	31.46°N, 110.27°E	2950	Sep. 2019	0.24 ± 0.03	Lyu et al. (2021)
Greater Higgnan Mountains, China	50.43°N124.13°E	376	May 2011	0.22 ± 0.08	Lyu et al. (2013)
Mt. Waliguan, China	36.28°N, 100.9°E	3816	Apr.-May 2003	0.18 ± 0.28	Xue et al. (2013)
Qinghai Lake, China	36.98°N, 99.91°E	3576	Apr. & Aug. 2010	0.18 ± 0.14	Lyu et al. (2013)
Mt. Jianfeng, China	18.67°N, 108.82°E	830	Apr.-May 2004	0.17 ± 0.44	Tang et al. (2009)
Nanling Mountains, China	**24.7°N, 112.9°E**	**1690**	**Oct.- Nov. 2016**	**0.16 ± 0.20**	**This study**
Mt. Tengchong, China	24.95°N, 98.48°E	1960	Apr.-May 2004	0.16 ± 0.10	Tang et al. (2009)
Mt. Moshi Daban, China	37.59°N, 101.29°E	3295	Sep.-Oct. 2013	0.12 ± 0.05	Zhao et al. (2020)
Mt. Wudang, China	32.45°N, 111.07°E	864	May- Jun. 2018	0.07 ± 0.04	Li et al. (2021)
Mt. Fuji, Japan	35.37°N, 138.73°E	3776	Aug. 2016	0.19 ± 0.09	Ou-Yang et al. (2017)
Mediterranean Stone Pine Forest, Spain	37.10°N, 6.7°W	12	Nov.-Dec. 2008	0.16 ± 0.24	Song et al. (2011)
Hyytiälä, Finland	61.85°N, 24.28°E	181	Sep.-Nov. 2000–2002	0.14 ± 0.12	Hakola et al. (2003)
Mt. Kleiner Feldberg, Germany	50.22°N, 8.45°E	850	Aug.-Sep. 2011	0.13	Sobanski et al. (2017)
Mt. Whiteface, USA	44.37°N, 73.9°W	1500	Jul. 1994	0.11	Khwaja and Narang (2008)
Valderejo Natural Park, Basque	42.87°N, 3.22°W	900	2003–2004	0.10 ± 0.14	Navazo et al. (2008)
Manitou Experimental Forest, USA	39.1°N, 105.1°W	2286	Aug. 2008	0.09 ± 0.06	Nakashima et al. (2014)
Cape Corse, France	42.97°N, 9.38°E	533	Jul. - Aug. 2013	0.08 ± 0.07	Michoud et al. (2017)
Cape Point, South Africa	34.5°S, 18.2°E	230	Jul. - Nov. 2017	0.06 ± 0.17	Kuyper et al. (2020)
Mt. Cimone, Italy	44.2°N, 10.7°E	2165	2010–2014	0.06	Lo Vullo et al. (2016)
Mt. Appalachian, USA	36.21°N, 81.69°W	1100	Jun. - Jul. 2013	0.06 ± 0.05	Link et al. (2015)
Cyprus island, Cyprus	35.03°N, 33.05°E	532	Mar. 2015	0.05	Debevec et al. (2017)
Amazon, Brazil	2.15°S, 59.01°W	80	2012–2013	0.03	Paralovo et al. (2016)
Jungfraujoch, Swiss	46.55°N, 7.98°E	3580	Oct.- Nov. 2015	0.01 ± 0.01	Balzani Lööv et al. (2008)

*Unpublished data supported by Prof. Hai Guo of Hong Kong Polytechnic University.

lower than expected. Three mountainous forests located in southern China, namely, Mt. Dinghu, Mt. Tai Mo Shan, and Mt. Lushan, presented the first, second, and fifth-highest toluene concentrations, respectively (Table 1). Toluene levels at these sites were approximately 6–15 times higher than those at NM. The average value of toluene in this study was even lower than that at Mt. Waliguan, a baseline Global Atmospheric Watch (GAW) station in the northeastern Tibetan Plateau region of China. Considering the strong atmospheric oxidative capacity in southern China (Yan et al., 2019) and NM as a receptor forest for the PRD-outflowed plumes, the faster photochemical degradation might be responsible for the unexpected low toluene, which requires further investigation.

The diurnal pattern of T/B ratios in NM was similar to other background sites (Fig. 2). The T/B ratios retained higher values, with a maximum value of 2.9 ± 3.4 ppbv·ppbv^{-1} before 9:00, then decreased to the lowest value of 1.1 ± 1.0 ppbv·ppbv^{-1} in the afternoon, with photochemical consumption induced by OH radicals. Compared with other background atmospheres in China, the diurnal profiles of the T/B ratios in this study were in good consistency with those observed at Shangdianzi (SDZ) in northern China and Hok Tsui (HT) in southern China. The ratios at Jinyunshan (JYS) in southwestern China showed insignificantly diurnal variations but also decreased slightly during the daytime. The toluene degradation rate, as ΔLn(T/B)/Δt in NM was 0.1 ppbv·ppbv^{-1}·h^{-1}, which is 2–5 times faster than that of HT, SDZ, and JYS, with values of 0.05, 0.04 and 0.02 ppbv·ppbv^{-1}·h^{-1}, respectively. The comparative results provide a reasonable explanation for the decidedly low toluene content in NM.

The OH concentrations in NM simulated by MCM was compared with those reported at other background sites to investigate the faster degradation rate of toluene in NM. The OH levels in NM were generally higher than most previously reported values at other background sites (Table 2). During the campaign, the daily maxima of the simulated OH levels in NM ranged from 7.5 to 18.0 × 10^6 molecule cm^{-3}, with an average daily peak value of (13.0 ± 3.0) × 10^6 molecule cm^{-3}, which was even comparable to the mean peak value in summer ((14.4 ± 0.8) × 10^6 molecule cm^{-3}) (Gong et al., 2018). Furthermore, these values were close to the highest oxidant levels (15.5 × 10^6 molecule cm^{-3}) reported at Backgarden, a background site in southern China. Given the weaker solar radiation and lower temperature in autumn, special attention should be paid to the unique mechanisms for maintaining OH levels in NM during this season.

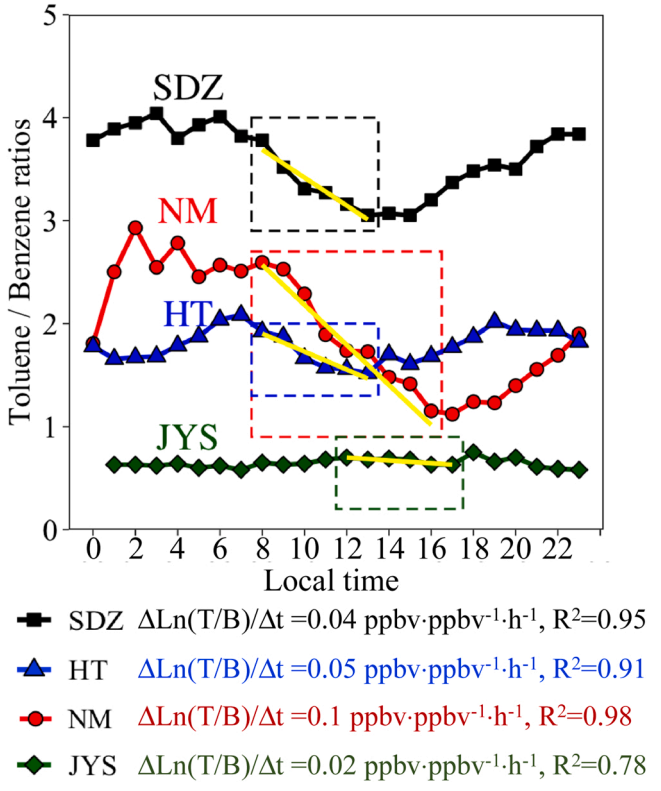

Fig. 2. Diurnal variations of toluene/benzene ratios observed at the Nanling Mountains (NM, in south China) and other background sites, including Shangdianzi (SDZ) in northern China, Hok Tsui (HT) in southern China and Jinyushan (JYS) in southwestern China. References are listed in Table 1. ΔLn (T/B)/Δt with R^2 for indicating degradation rate of toluene for each site have also been presented. Yellow lines indicate linear degradation for toluene oxidation. (For interpretation of the references to colour in this figure legend, the reader is referred to the web version of this article.)

Table 2
Daytime OH concentrations at the Nanling Mountains and other background sites.

Site	Date	OH (×10^6 molecule cm^{-3})	Methods	References
Nanling Mountains, China	Oct.-Nov. 2016	7.5–18.0[a]	Modelling	This study
Nanling Mountains, China	Jun.-Aug. 2016	14.4 ± 0.8[b]	Modelling	Gong et al. (2018)
Back Garden, China	Jul. 2006	15.0[b]	Measurement	Hofzumahaus et al. (2009)
Mt. Mang, China	Sep.-Oct. 2007	0.4–14.2[a]	Measurement	Suthawaree et al. (2012)
Tai Mao Shan, China	Sep.-Nov. 2010	3.9 ± 0.7[c]	Modelling	Guo et al. (2013)
Wanshan Island, China	Aug.-Nov. 2013	4.7–9.2[b]	Modelling	Wang et al. (2018)
Mt. Tai, China	Jun. 2006	5.4–5.7[b]	Modelling	Kanaya et al. (2009)
Shennongjia, China	Sep. 2019	1.1[b]	Modelling	Lyu et al. (2021)
Agrafa mountains, Greece	Jul.-Aug. 1997	4.0–12.0[a]	Measurement	Creasey et al. (2001)
Manitou Experimental Forest, US	Aug. 2010	3.0–10.0[a]	Measurement	Wolfe et al. (2014)
Jülich, Germany	Summer 2003	4.0–9.0[a]	Measurement	Kleffmann et al. (2005)
Amazon, Brazil	Oct. 2005	5.6 ± 1.9	Measurement	Lelieveld et al. (2008)
Sierra Nevada mountains, US	Summer 1999	9.0[b]	Calculation	Dreyfus et al. (2002)
Hohenpeissenberg, Germany	Jun. 2000	4.5–7.4[a]	Measurement	Handisides et al. (2003)
Central Valley, US	May 2011	4.0–7.0[b]	Calculation	Karl et al. (2013)
Hyytiälä, Finland	Summer 2010	1.5–2.0[a]	Measurement	Hens et al. (2014)
Mt. Kleiner Feldberg, Germany	Aug.-Sep. 2011	3.0[b]	Measurement	Sobanski et al. (2017)
Mace Head, Ireland	Jun. 1999	2.6 ± 0.5[b]	Measurement	Berresheim et al. (2002)
Whiteface Mountain, US	Summer 2002	2.6[b]	Measurement	Ren et al. (2006)
Tasmania, Australia	Jan.-Feb. 1999	2.6–3.6[a]	Measurement	Sommariva et al. (2004)
Talladega National Forest, US	Jun.-Jul. 2013	1.0[b]	Modelling	Feiner et al. (2016)

a denotes the range of daytime maxima, b indicates average values of daytime maxima, c denotes mean values during daytime, and d is the median for maxima values at noon.

3.2. Impact of urban plumes on the atmospheric chemistry in NM

Observational evidence has revealed a significantly elevated atmospheric oxidative capacity over downwind forests under the disturbance of urban pollution plumes (Liu et al., 2018). More abundant oxygenated VOCs over NM in the presence of PRD outflow were reported in our previous study (Lv et al., 2019). To investigate how urban plumes disturb the concentrations of toluene and secondary products in NM, an episode (October 24–28) with a southern prevailing wind and an episode (November 1–3) with a northern prevailing wind were selected (Fig. S1). Given the relatively short lifetime of toluene (approximately 24 h) (Cabrera-Perez et al., 2016), 24-h backward trajectories were analyzed (Text S1). The results confirmed that air masses in the first and second episodes mainly traversed the PRD region and central China, respectively (Fig. 1). A clean period (October 16–18) with significantly less anthropogenic pollutants (toluene = 0.02 ± 0.01 ppbv) (Table S1) was selected for comparison. During the clean period, the air masses arriving in NM were predominantly from the eastern parts of Guangdong and Jiangxi provinces. The clean period and first and second episodes were named as Clean Case, PRD Case, and central China (CC) Case, respectively.

Fig. 3 illustrates the diurnal variations in toluene and benzaldehyde concentrations with other parameters for the three cases. More toluene was transported into NM by the PRD outflow, resulting in an increased toluene concentration in PRD Case to an average of 0.33 ± 0.32 ppbv (Table S1). However, the toluene values in PRD Case remained lower than those at other sites in southern China (Table 1). Toluene in PRD Case decreased from 0.46 ± 0.51 ppbv at 11:00 to the lowest value of 0.13 ± 0.08 ppbv at 16:00, which was down to the same level as in CC Case. In contrast, the daily toluene in the other cases had lower values ($p < 0.01$) and degraded slowly during the daytime. According to previous studies by Wang et al. (2021), the upslope flow with the exchange of the planetary boundary layer lead to lower values of O_3 during daytime at NM. However, considering the slower decrease in daytime toluene in the other two cases, the contribution of the dilution effect to the accelerated toluene degradation in PRD Case might be limited. O_x ($O_3 + NO_2$) was recognized as the 'total oxidant' (Lu et al., 2010), higher O_x values ($p < 0.01$) were observed in PRD Case, suggesting a more intense atmospheric oxidative capacity in PRD Case than in the other cases. Therefore, the accelerated toluene degradation in PRD Case should have been dominated by stronger photochemical oxidation rather than physical processes.

Daytime benzaldehyde concentrations were significantly enhanced by PRD plumes in the presence of large amounts of toluene and oxidants, with maximum values approximately 240% and 56% higher than the background level (the lowest value observed in this study) and CC Case, respectively. Notably, the similar nighttime benzaldehyde levels in the PRD and CC Cases suggest comparable contributions of long-range transport. Furthermore, when considering the short lifetime of benzaldehyde (approximately 2.4 h) (Cabrera-Perez et al., 2016), the daytime elevation of benzaldehyde in NM under the influence of PRD outflows could be mainly because of secondary formation rather than long-range transport. In addition to benzaldehyde, air masses from the PRD region also contributed to significantly higher daytime O_3 than Clean Case and CC Case ($p < 0.01$). Notably, both benzaldehyde and O_3 are regarded as toxicants in forest ecosystems (Lindroth, 2010; Lohonyai et al., 2019).

A significant isoprene elevation was observed during the day in PRD Case ($p < 0.01$), while the Clean and CC Cases showed lower values of isoprene. Given the short lifetime of isoprene (approximately 1 −2 h) (Wennberg et al., 2018), this phenomenon could be explained by more isoprene emissions from plants with elevated temperatures ($p < 0.01$, Fig. 3**j**), induced by warmer air masses transported from the south. In terms of NO_x, PRD Case showed comparable values to those of CC Case ($p > 0.1$). Significantly elevated levels of CO and benzene were found in CC Case ($p < 0.01$), indicating that more CO and benzene were transported from central China. These phenomena are consistent with the spatial distributions of CO and benzene in China, with higher levels in central China and lower levels in southern China (Liu et al., 2019; Yan et al., 2019).

In conclusion, the present results suggest that the atmospheric chemistry in NM has been seriously affected by outflow from the PRD and central China. In particular, the PRD pollution plumes are more likely to induce rapid toluene degradation and secondary product formation by strengthening atmospheric oxidative capacity over NM, which requires further analysis.

3.3. Toluene degradation accelerated by the elevated OH radicals in PRD plumes

Fig. 4 shows the diurnal variations in T/B ratios and the daytime degradation rate ($\Delta Ln(T/B)/\Delta t$) for the three cases. In PRD Case, the daytime T/B ratios presented a significant drop, with a mean $\Delta Ln(T/B)/\Delta t$ up to 0.16 ppbv ppbv^{-1} h^{-1}, which was faster than Clean Case (0.09 ppbv ppbv^{-1} h^{-1}) and CC Case (0.07 ppbv ppbv^{-1} h^{-1}, $R^2 = 1$) by 80% and 130%, respectively. The degradation rate of toluene in PRD Case was very rapid, and approximately 8 times that in JYS. These results demonstrated a relatively faster degradation rate of toluene in NM under the influence of the PRD-polluted air masses.

Fig. 5 presents the MCM-simulated OH concentrations in NM for the Clean, PRD and the CC Cases. The average of the simulated daily OH peak concentrations reached (15.8 ± 2.2) × 10^6 molecule cm^{-3} in PRD Case, which was enhanced by more than 30% compared to the maximum value in Clean Case. In contrast, the mean peak value was reduced to (9.1 ± 1.3) × 10^6 molecule cm^{-3} under the influence of the plumes from central China, which was approximately 25% less than the simulated value in Clean Case.

The OH concentrations in forests are generally constrained by several factors, including NO_x, O_3, BVOCs, and CO (Hens et al., 2014). Amplified OH concentrations with increased NO_x concentrations in urban pollution plumes were found in the Amazon, which is the largest humid tropical forest in the world (Liu et al., 2018). However, the comparable NO_x in the PRD and the CC Cases suggests that the elevation of OH concentrations in the PRD Case may not be induced by changes in NO_x. Kubistin et al. (2010) found that OH radicals produced from O_3 photolysis and ozonolysis reactions may also play a key role in strengthening the atmospheric oxidative capacity of forests. This was supported by our observation of elevated O_3 in the PRD plumes, suggesting a likely greater contribution of O_3 photochemistry to OH formation in NM. In addition, recent studies have demonstrated that, rather than depleting OH radicals, isoprene photochemistry over forests can promote atmospheric oxidative capacity by efficient OH recycling (Lelieveld et al., 2008). This point was also supported by the fact that the diurnal pattern of isoprene, which usually shows a peak value at noon due to the strong emissions by plants, showed a trough at this time in PRD Case (Fig. 3**e**). Overall, the characteristics of O_3 and isoprene likely suggest evidence of OH generation from isoprene ozonolysis reactions, an important source of OH in the PRD plumes. Furthermore, a sharp decrease in OH levels because of increasing CO concentrations has been reported in a boreal forest (Hens et al., 2014) and therefore, the apparently elevated CO should be responsible for lower OH concentrations in the central China plumes.

4. Conclusions and implications

In this study, toluene and its oxidation product, benzaldehyde, were measured in NM, the receptor forest surrounding the PRD region in China. Unexpectedly lower levels of toluene were observed compared to other background sites in China. The quantitative assessment revealed that the fastest degradation rate for toluene in the Chinese background sites was found in NM. Furthermore, the accelerated transformations of toluene and the subsequent enhanced formation of secondary products, some of which are toxic to the forest ecosystem, have been reported in

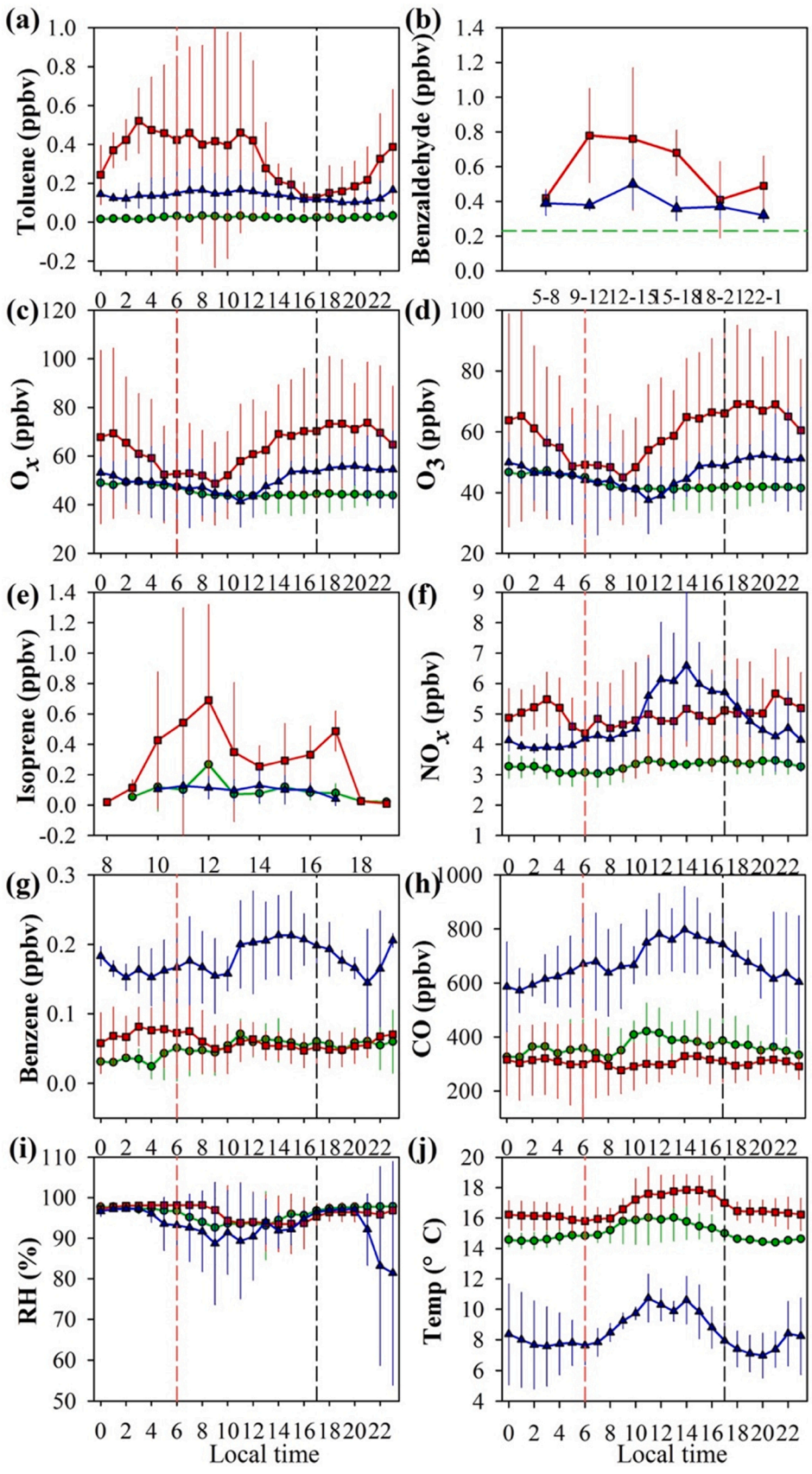

Fig. 3. Diurnal variations of hourly averaged values (± standard deviations) for toluene (a), benzaldehyde (n = 42) (b), O_x (c), O_3 (d), isoprene (e), NO_x (f), benzene (g), CO (h), RH (i) and Temp. (j) in Clean Case, PRD Case, and central China (CC) Case in the Nanling Mountains. The green dotted line (b) indicates the background level of benzaldehyde in the Nanling Mountains. (For interpretation of the references to colour in this figure legend, the reader is referred to the web version of this article.)

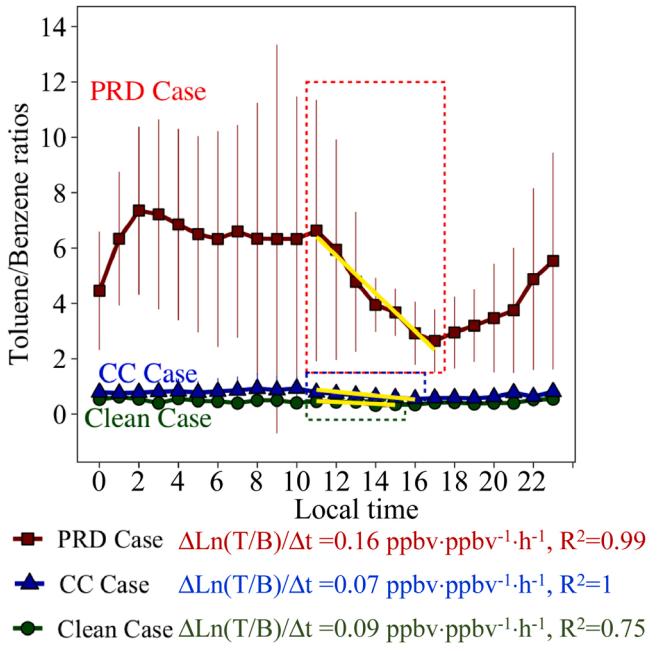

Fig. 4. Diurnal variations of toluene/benzene ratios for Clean Case, PRD Case and central China (CC) Case in the Nanling Mountains. ΔLn(T/B)/Δt with R^2 indicates the degradation rate of toluene for each case. Yellow lines indicate linear degradation for toluene oxidation. Error bars are the standard deviations. (For interpretation of the references to colour in this figure legend, the reader is referred to the web version of this article.)

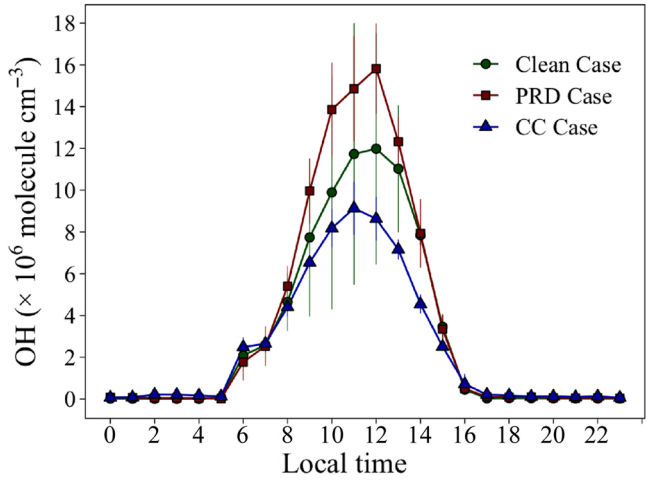

Fig. 5. Comparisons of OH radicals simulated by MCM during Clean Case, PRD Case and central China (CC) Case. Error bars are the standard deviations.

the presence of the PRD plumes. This phenomenon can be explained by the enhancement of atmospheric oxidative capacity over NM.

The results of this study provide strong evidence that massive emissions of toxic toluene in urban agglomerations have a significant impact on the atmospheric chemistry of surrounding forests. As a response, receptor forests can accelerate the degradation of transported toxicants because of their strong atmospheric oxidative capacity. Therefore, the preservation and plantation of forests are important for ensuring environmental safety, given the role of forests as 'air-cleaners' by accelerating the sink of toxic substances. Further studies are necessary to gain a more comprehensive understanding of the clearance mechanisms of anthropogenic toxicants over forests, which are important for regional and global air pollution control.

CRediT authorship contribution statement

Qinqin Li: Conceptualization, Methodology, Formal analysis, Investigation, Writing, Visualization. **Daocheng Gong:** Editing, Methodology, Writing. **Yu Wang:** Methodology, Software. **Hao Wang:** Methodology, Data curation, Editing, Project administration, Funding acquisition. **Wenlu Wang & Gengchen Wu:** Formal analysis. **Hai Guo:** MCM model support, Data curation. **Boguang Wang:** Conceptualization, Supervision, Funding acquisition.

Declaration of Competing Interest

The authors declare that they have no known competing financial interests or personal relationships that could have appeared to influence the work reported in this paper.

Acknowledgements

This work was supported by the National Natural Science Foundation of China (NSFC) Projects (42077190, 41877370 and 42005080); the Science and Technology Planning Project of Guangdong Province of China (2019B121202002); Guangdong Innovative and Entrepreneurial Research Team Program (2016ZT06N263); and China Postdoctoral Science Foundation (2020M673059). We thank Prof. Hai Guo of the Hong Kong Polytechnic University for the assistance of the simulation by the PBM-MCM model.

Appendix A. Supporting information

Supplementary data associated with this article can be found in the online version at doi:10.1016/j.ecoenv.2021.113126.

References

Atkinson, R., Arey, J., 2003. Atmospheric degradation of volatile organic compounds. Chem. Rev. 103, 4605–4638.

Balzani Lööv, J.M., Henne, S., Legreid, G., Staehelin, J., Reimann, S., Prévôt, A.S.H., Steinbacher, M., Vollmer, M.K., 2008. Estimation of background concentrations of trace gases at the Swiss Alpine site Jungfraujoch (3580 m asl). J. Geophys. Res. Atmos. 113.

Berresheim, H., Elste, T., Tremmel, H.G., Allen, A.G., Hansson, H.-C., Rosman, K., Dal Maso, M., Mäkelä, J.M., Kulmala, M., O'Dowd, C.D., 2002. Gas-aerosol relationships of H_2SO_4, MSA, and OH: observations in the coastal marine boundary layer at Mace Head, Ireland. J. Geophys. Res. Atmos. 107. PAR 5-1-PAR 5-12.

Cabrera-Perez, D., Taraborrelli, D., Sander, R., Pozzer, A., 2016. Global atmospheric budget of simple monocyclic aromatic compounds. Atmos. Chem. Phys. 16, 6931–6947.

Chen, L., Bao, K., Li, K., Lv, B., Bao, Z., Chao, L., Wu, X., Zheng, C., Gao, X., Cen, K., et al., 2017. Ozone and secondary organic aerosol formation of toluene/NO_x irradiations under complex pollution scenarios. Aerosol and Air Quality Research. https://doi.org/10.4209/aaqr.2017.05.0179.

Creasey, D.J., Heard, D.E., Lee, J.D., 2001. OH and HO_2 measurements in a forested region of north-western Greece. Atmos. Environ. 35, 4713–4724.

Custódio, D., Guimarães, C.S., Varandas, L., Arbilla, G., 2010. Pattern of volatile aldehydes and aromatic hydrocarbons in the largest urban rainforest in the Americas. Chemosphere 79, 1064–1069.

de Gouw, J.A., Brock, C.A., Atlas, E.L., Bates, T.S., Fehsenfeld, F.C., Goldan, P.D., Holloway, J.S., Kuster, W.C., Lerner, B.M., Matthew, B.M., Middlebrook, A.M., Onasch, T.B., Peltier, R.E., Quinn, P.K., Senff, C.J., Stohl, A., Sullivan, A.P., Trainer, M., Warneke, C., Weber, R.J., Williams, E.J., 2008. Sources of particulate matter in the northeastern United States in summer: 1. Direct emissions and secondary formation of organic matter in urban plumes. J. Geophys. Res. Atmos. 113.

Debevec, C., Sauvage, S., Gros, V., Sciare, J., Pikridas, M., Stavroulas, I., Salameh, T., Leonardis, T., Gaudion, V., Depelchin, L., Fronval, I., Sarda-Esteve, R., Baisnée, D., Bonsang, B., Savvides, C., Vrekoussis, M., Locoge, N., 2017. Origin and variability in volatile organic compounds observed at an Eastern Mediterranean background site (Cyprus). Atmos. Chem. Phys. 17, 11355–11388.

Dreyfus, G.B., Schade, G.W., Goldstein, A.H., 2002. Observational constraints on the contribution of isoprene oxidation to ozone production on the western slope of the Sierra Nevada, California. J. Geophys. Res. Atmos. 1–17 (ACH 1-1-ACH).

Fang, X.K., Shao, M., Stohl, A., Zhang, Q., Zheng, J.Y., Guo, H., Wang, C., Wang, M., Ou, J.M., Thompson, R.L., Prinn, R.G., 2016. Top-down estimates of benzene and toluene emissions in the Pearl River Delta and Hong Kong, China. Atmos. Chem. Phys. 16, 3369–3382.

Feiner, P.A., Brune, W.H., Miller, D.O., Zhang, L., Cohen, R.C., Romer, P.S., Goldstein, A. H., Keutsch, F.N., Skog, K.M., Wennberg, P.O., Nguyen, T.B., Teng, A.P., DeGouw, J., Koss, A., Wild, R.J., Brown, S.S., Guenther, A., Edgerton, E., Baumann, K., Fry, J.L., 2016. Testing atmospheric oxidation in an Alabama Forest. J. Atmos. Sci. 73, 4699–4710.

Gong, D., Wang, H., Zhang, S., Wang, Y., Liu, S.C., Guo, H., Shao, M., He, C., Chen, D., He, L., Zhou, L., Morawska, L., Zhang, Y., Wang, B., 2018. Low-level summertime isoprene observed at a forested mountaintop site in southern China: implications for strong regional atmospheric oxidative capacity. Atmos. Chem. Phys. 18, 14417–14432.

Guo, H., Ling, Z.H., Cheung, K., Jiang, F., Wang, D.W., Simpson, I.J., Barletta, B., Meinardi, S., Wang, T.J., Wang, X.M., Saunders, S.M., Blake, D.R., 2013. Characterization of photochemical pollution at different elevations in mountainous areas in Hong Kong. Atmos. Chem. Phys. 13, 3881–3898.

Hakola, H., Tarvainen, V., Laurila, T., Hiltunen, V., Hellén, H., Keronen, P., 2003. Seasonal variation of VOC concentrations above a boreal coniferous forest. Atmos. Environ. 37, 1623–1634.

Han, T., Ma, Z., Xu, W., Qiao, L., Li, Y., He, D., Wang, Y., 2020. Characteristics and source implications of aromatic hydrocarbons at urban and background areas in Beijing, China. Sci. Total Environ. 707, 136083.

Handisides, G.M., Plass-Dülmer, C., Gilge, S., Bingemer, H., Berresheim, H., 2003. Hohenpeissenberg Photochemical Experiment (HOPE 2000): measurements and photostationary state calculations of OH and peroxy radicals. Atmos. Chem. Phys. 3, 1565–1588.

Hens, K., Novelli, A., Martinez, M., Auld, J., Axinte, R., Bohn, B., Fischer, H., Keronen, P., Kubistin, D., Nölscher, A.C., Oswald, R., Paasonen, P., Petäjä, T., Regelin, E., Sander, R., Sinha, V., Sipilä, M., Taraborrelli, D., Tatum Ernest, C., Williams, J., Lelieveld, J., Harder, H., 2014. Observation and modelling of HOx radicals in a boreal forest. Atmos. Chem. Phys. 14, 8723–8747.

Hofzumahaus, A., Rohrer, F., Lu, K., Bohn, B., Brauers, T., Chang, C., Fuchs, H., Holland, F., Kita, K., Kondo, Y., 2009. Amplified trace gas removal in the troposphere. Science 324, 1702–1704.

Hong, Z., Li, M., Wang, H., Xu, L., Hong, Y., Chen, J., Chen, J., Zhang, H., Zhang, Y., Wu, X., Hu, B., Li, M., 2019. Characteristics of atmospheric volatile organic compounds (VOCs) at a mountainous forest site and two urban sites in the southeast of China. Sci. Total Environ. 657, 1491–1500.

Kanaya, Y., Pochanart, P., Liu, Y., Li, J., Tanimoto, H., Kato, S., Suthawaree, J., Inomata, S., Taketani, F., Okuzawa, K., Kawamura, K., Akimoto, H., Wang, Z.F., 2009. Rates and regimes of photochemical ozone production over Central East China in June 2006: a box model analysis using comprehensive measurements of ozone precursors. Atmos. Chem. Phys. 9, 7711–7723.

Karl, T., Misztal, P.K., Jonsson, H.H., Shertz, S., Goldstein, A.H., Guenther, A., 2013. Airborne flux measurements of BVOCs above Californian Oak Forests: experimental investigation of surface and entrainment fluxes, OH densities, and damköhler numbers. J. Atmos. Sci. 70, 3277–3287.

Khan, M.A.H., Schlich, B.-L., Jenkin, M.E., Cooke, M.C., Derwent, R.G., Neu, J.L., Percival, C.J., Shallcross, D.E., 2021. Changes to simulated global atmospheric composition resulting from recent revisions to isoprene oxidation chemistry. Atmos. Environ. 244, 117914.

Khwaja, H.A., Narang, A., 2008. Carbonyls and non-methane hydrocarbons at a rural mountain site in northeastern United States. Chemosphere 71, 2030–2043.

Kleffmann, J., Gavriloaiei, T., Hofzumahaus, A., Holland, F., Koppmann, R., Rupp, L., Schlosser, E., Siese, M., Wahner, A., 2005. Daytime formation of nitrous acid: a major source of OH radicals in a forest. Geophys. Res. Lett. 32.

Kubistin, D., Harder, H., Martinez, M., Rudolf, M., Sander, R., Bozem, H., Eerdekens, G., Fischer, H., Gurk, C., Klüpfel, T., Königstedt, R., Parchatka, U., Schiller, C.L., Stickler, A., Taraborrelli, D., Williams, J., Lelieveld, J., 2010. Hydroxyl radicals in the tropical troposphere over the Suriname rainforest: comparison of measurements with the box model MECCA. Atmos. Chem. Phys. 10, 9705–9728.

Kuyper, B., Wingrove, H., Lesch, T., Labuschagne, C., Say, D., Martin, D., Young, D., Khan, M.A.H., O'Doherty, S., Davies-Coleman, M.T., Shallcross, D.E., 2020. Atmospheric toluene and benzene mole fractions at Cape Town and Cape Point and an estimation of the hydroxyl radical concentrations in the air above the Cape Peninsula, South Africa. ACS Earth Space Chem. 4, 24–34.

Lelieveld, J., Butler, T.M., Crowley, J.N., Dillon, T.J., Fischer, H., Ganzeveld, L., Harder, H., Lawrence, M.G., Martinez, M., Taraborrelli, D., Williams, J., 2008. Atmospheric oxidation capacity sustained by a tropical forest. Nature 452, 737–740.

Li, J., Zhai, C., Yu, J., Liu, R., Li, Y., Zeng, L., Xie, S., 2018. Spatiotemporal variations of ambient volatile organic compounds and their sources in Chongqing, a mountainous megacity in China. Sci. Total Environ. 627, 1442–1452.

Li, L., Wang, X., 2012. Seasonal and diurnal variations of atmospheric non-methane hydrocarbons in Guangzhou. China Int. J. Environ. Res. Public Health 9, 1859–1873.

Li, Y., Gao, R., Xue, L., Wu, Z., Yang, X., Gao, J., Ren, L., Li, H., Ren, Y., Li, G., Li, C., Yan, Z., Hu, M., Zhang, Q., Xu, Y., 2021. Ambient volatile organic compounds at Wudang Mountain in Central China: characteristics, sources and implications to ozone formation. Atmos. Res. 250, 105359.

Lin, Y., Gong, D., Lv, S., Ding, Y., Wu, G., Wang, H., Li, Y., Wang, Y., Zhou, L., Wang, B., 2019. Observations of high levels of ozone-depleting CFC-11 at a remote mountain-top site in Southern China. Environ. Sci. Technol. Lett. 6, 114–118.

Lindroth, R.L., 2010. Impacts of elevated atmospheric CO_2 and O_3 on forests: phytochemistry, trophic interactions, and ecosystem dynamics. J. Chem. Ecol. 36, 2–21.

Link, M., Zhou, Y., Taubman, B., Sherman, J., Morrow, H., Krintz, I., Robertson, L., Cook, R., Stocks, J., West, M., Sive, B.C., 2015. A characterization of volatile organic compounds and secondary organic aerosol at a mountain site in the Southeastern United States. J. Atmos. Chem. 72, 81–104.

Liu, D., Di, B., Luo, Y., Deng, X., Zhang, H., Yang, F., Grieneisen, M.L., Zhan, Y., 2019. Estimating ground-level CO concentrations across China based on the national monitoring network and MOPITT: potentially overlooked CO hotspots in the Tibetan Plateau. Atmos. Chem. Phys. 19, 12413–12430.

Liu, Y., Seco, R., Kim, S., Guenther, A., Goldstein, A.H., Keutsch, F.N., Springston, S.R., Watson, T., Artaxo, P., Souza, R.A.F., 2018. Isoprene photo-oxidation products quantify the effect of pollution on hydroxyl radicals over Amazonia. Sci. Adv. 4.

Lo Vullo, E., Furlani, F., Arduini, J., Giostra, U., Graziosi, F., Cristofanelli, P., Williams, M.L., Maione, M., 2016. Anthropogenic non-methane volatile hydrocarbons at Mt. Cimone (2165 m a.s.l., Italy): impact of sources and transport on atmospheric composition. Atmos. Environ. 140, 395–403.

Lohonyai, Z., Vuts, J., Kárpáti, Z., Koczor, S., Domingue, M.J., Fail, J., Birkett, M.A., Tóth, M., Imrei, Z., 2019. Benzaldehyde: an alfalfa-related compound for the spring attraction of the pest weevil Sitona humeralis (Coleoptera: Curculionidae). Pest Manag. Sci. 75, 3153–3159.

Lu, K., Guo, S., Tan, Z., Wang, H., Shang, D., Liu, Y., Li, X., Wu, Z., Hu, M., Zhang, Y., 2018. Exploring atmospheric free-radical chemistry in China: the self-cleansing capacity and the formation of secondary air pollution. Natl. Sci. Rev. 6, 579–594.

Lu, K., Zhang, Y., Su, H., Brauers, T., Chou, C.C., Hofzumahaus, A., Liu, S.C., Kita, K., Kondo, Y., Shao, M., Wahner, A., Wang, J., Wang, X., Zhu, T., 2010. Oxidant (O_3 + NO_2) production processes and formation regimes in Beijing. J. Geophys. Res. Atmos. 115.

Lv, S., Gong, D., Ding, Y., Lin, Y., Wang, H., Ding, H., Wu, G., He, C., Zhou, L., Liu, S., Ristovski, Z., Chen, D., Shao, M., Zhang, Y., Wang, B., 2019. Elevated levels of glyoxal and methylglyoxal at a remote mountain site in southern China: prompt in-situ formation combined with strong regional transport. Sci. Total Environ. 672, 869–882.

Lyu, X., Guo, H., Zhang, W., Cheng, H., Yao, D., Lu, H., Zhang, L., Zeren, Y., Liu, X., Qian, Z., Wang, S., 2021. Ozone and its precursors in a high-elevation and highly forested region in central China: origins, in-situ photochemistry and implications of regional transport. Atmos. Environ. 259, 118540.

Lyu, Y.-b, Tan, L., Teng, E., Wang, C., Lyu, T., Liang, X., 2013. Concentration levels and composition characteristics of VOCs at the background locations in China (in Chinese). Environ. Chem. 32.

Martin, S.T., Artaxo, P., Machado, L., Manzi, A.O., Souza, R.A.F., Schumacher, C., Wang, J., Biscaro, T., Brito, J., Calheiros, A., Jardine, K., Medeiros, A., Portela, B., Sá, S.S. d, Adachi, K., Aiken, A.C., Albrecht, R., Alexander, L., Andreae, M.O., Barbosa, H.M.J., Buseck, P., Chand, D., Comstock, J.M., Day, D.A., Dubey, M., Fan, J., Fast, J., Fisch, G., Fortner, E., Giangrande, S., Gilles, M., Goldstein, A.H., Guenther, A., Hubbe, J., Jensen, M., Jimenez, J.L., Keutsch, F.N., Kim, S., Kuang, C., Laskin, A., McKinney, K., Mei, F., Miller, M., Nascimento, R., Pauliquevis, T., Pekour, M., Peres, J., Petäjä, T., Pöhlker, C., Pöschl, U., Rizzo, L., Schmid, B., Shilling, J.E., Dias, M.A.S., Smith, J.N., Tomlinson, J.M., Tóta, J., Wendisch, M., 2017. The Green Ocean Amazon experiment (GoAmazon2014/5) observes pollution affecting gases, aerosols, clouds, and rainfall over the rain forest. Bull. Am. Meteorol. Soc. 98, 981–997.

Michoud, V., Sciare, J., Sauvage, S., Dusanter, S., Léonardis, T., Gros, V., Kalogridis, C., Zannoni, N., Féron, A., Petit, J.E., Crenn, V., Baisnée, D., Sarda-Estève, R., Bonnaire, N., Marchand, N., DeWitt, H.L., Pey, J., Colomb, A., Gheusi, F., Szidat, S., Stavroulas, I., Borbon, A., Locoge, N., 2017. Organic carbon at a remote site of the western Mediterranean Basin: sources and chemistry during the ChArMEx SOP2 field experiment. Atmos. Chem. Phys. 17, 8837–8865.

Mo, Z., Shao, M., Liu, Y., Xiang, Y., Wang, M., Lu, S., Ou, J., Zheng, J., Li, M., Zhang, Q., Wang, X., Zhong, L., 2018. Species-specified VOC emissions derived from a gridded study in the Pearl River Delta, China. Sci. Rep. 8, 2963.

Nakashima, Y., Kato, S., Greenberg, J., Harley, P., Karl, T., Turnipseed, A., Apel, E., Guenther, A., Smith, J., Kajii, Y., 2014. Total OH reactivity measurements in ambient air in a southern Rocky mountain ponderosa pine forest during BEACHON-SRM08 summer campaign. Atmos. Environ. 85, 1–8.

Navazo, M., Durana, N., Alonso, L., Gómez, M.C., García, J.A., Ilardia, J.L., Gangoiti, G., Iza, J., 2008. High temporal resolution measurements of ozone precursors in a rural background station. A two-year study. Environ. Monit. Assess. 136, 53–68.

Okamoto, S., Tanimoto, H., 2016. A review of atmospheric chemistry observations at mountain sites. Prog. Earth Planet Sci. 3, 34.

Ou-Yang, C.-F., Chang, C.-C., Wang, J.-L., Shimada, K., Hatakeyama, S., Kato, S., Chiu, J.-Y., Sheu, G.-R., Lin, N.-H., 2017. Characteristics of summertime volatile organic compounds in the lower free troposphere: background measurements at Mt. Fuji. Aerosol Air Qual. Res 17, 3037–3051.

Paralovo, S.L., Barbosa, C.G.G., Carneiro, I.P.S., Kurzlop, P., Borillo, G.C., Schiochet, M.F. C., Godoi, A.F.L., Yamamoto, C.I., de Souza, R.A.F., Andreoli, R.V., Ribeiro, I.O., Manzi, A.O., Kourtchev, I., Bustillos, J.O.V., Martin, S.T., Godoi, R.H.M., 2019. Observations of particulate matter, NO_2, SO_2, O_3, H_2S and selected VOCs at a semi-urban environment in the Amazon region. Sci. Total Environ. 650, 996–1006.

Paralovo, S.L., Borillo, G.C., Barbosa, C.G.G., Godoi, A.F.L., Yamamoto, C.I., de Souza, R. A.F., Andreoli, R.V., Costa, P.S., Almeida, G.P., Manzi, A.O., Pöhlker, C., Yáñez-Serrano, A.M., Kesselmeier, J., Godoi, R.H.M., 2016. Observations of atmospheric monoaromatic hydrocarbons at urban, semi-urban and forest environments in the Amazon region. Atmos. Environ. 128, 175–184.

Ren, X., Brune, W.H., Oliger, A., Metcalf, A.R., Simpas, J.B., Shirley, T., Schwab, J.J., Bai, C., Roychowdhury, U., Li, Y., Cai, C., Demerjian, K.L., He, Y., Zhou, X., Gao, H., Hou, J., 2006. OH, HO_2, and OH reactivity during the PMTACS–NY Whiteface Mountain 2002 campaign: observations and model comparison. J. Geophys. Res. Atmos. 111.

Saunders, S.M., Jenkin, M.E., Derwent, R.G., Pilling, M.J., 2003. Protocol for the development of the Master Chemical Mechanism, MCM v3 (Part A): tropospheric

degradation of non-aromatic volatile organic compounds. Atmos. Chem. Phys. 3, 161–180.
Sobanski, N., Thieser, J., Schuladen, J., Sauvage, C., Song, W., Williams, J., Lelieveld, J., Crowley, J.N., 2017. Day and night- time formation of organic nitrates at a forested mountain site in south-west Germany. Atmos. Chem. Phys. 17, 4115–4130.
Sommariva, R., Haggerstone, A.L., Carpenter, L.J., Carslaw, N., Creasey, D.J., Heard, D. E., Lee, J.D., Lewis, A.C., Pilling, M.J., Zádor, J., 2004. OH and HO_2 chemistry in clean marine air during SOAPEX-2. Atmos. Chem. Phys. 4, 839–856.
Song, W., Williams, J., Yassaa, N., Martinez, M., Carnero, J.A.A., Hidalgo, P.J., Bozem, H., Lelieveld, J., 2011. Winter and summer characterization of biogenic enantiomeric monoterpenes and anthropogenic BTEX compounds at a Mediterranean Stone Pine forest site. J. Atmos. Chem. 68, 233–250.
Song, Y., Shao, M., Liu, Y., Lu, S., Kuster, W., Goldan, P., Xie, S., 2007. Source apportionment of ambient volatile organic compounds in Beijing. Environ. Sci. Technol. 41, 4348–4353.
Suthawaree, J., Kato, S., Pochanart, P., Kanaya, Y., Akimoto, H., Wang, Z., Kajii, Y., 2012. Influence of Beijing outflow on Volatile Organic Compounds (VOC) observed at a mountain site in North China Plain. Atmos. Res. 111, 46–57.
Tang, J.H., Chan, L.Y., Chang, C.C., Liu, S., Li, Y.S., 2009. Characteristics and sources of non-methane hydrocarbons in background atmospheres of eastern, southwestern, and southern China. J. Geophys. Res. Atmos. 114.
Ting, M., Yue-si, W., Hong-hui, X., Jie, J., Fang-kun, W., Xiao-bin, X., 2009. A study of the atmospheric VOCs of Mount Tai in June 2006. Atmos. Environ. 43, 2503–2508.
Wang, Y., Guo, H., Zou, S., Lyu, X., Ling, Z., Cheng, H., Zeren, Y., 2018. Surface O_3 photochemistry over the South China Sea: application of a near-explicit chemical mechanism box model. Environ. Pollut. 234, 155–166.
Wang, Y., Shen, J., Wang, H., Wu, G., Chen, Y., Liu, T., Gong, D., Ou, J., Shi, Y., Zhang, T., He, C., Chen, D., Wang, B., 2021. Unexpected seasonal variations and high levels of ozone observed at the summit of Nanling Mountains: Impact of Asian monsoon on southern China. Atmos. Environ. 253, 118378.
Wennberg, P.O., Bates, K.H., Crounse, J.D., Dodson, L.G., McVay, R.C., Mertens, L.A., Nguyen, T.B., Praske, E., Schwantes, R.H., Smarte St, M.D., Clair, J.M., Teng, A.P., Zhang, X., Seinfeld, J.H., 2018. Gas-Phase reactions of isoprene and its major oxidation products. Chem. Rev. 118, 3337–3390.
Wolfe, G.M., Cantrell, C., Kim, S., Mauldin Iii, R.L., Karl, T., Harley, P., Turnipseed, A., Zheng, W., Flocke, F., Apel, E.C., Hornbrook, R.S., Hall, S.R., Ullmann, K., Henry, S. B., DiGangi, J.P., Boyle, E.S., Kaser, L., Schnitzhofer, R., Hansel, A., Graus, M., Nakashima, Y., Kajii, Y., Guenther, A., Keutsch, F.N., 2014. Missing peroxy radical sources within a summertime ponderosa pine forest. Atmos. Chem. Phys. 14, 4715–4732.
Wu, F., Yu, Y., Sun, J., Zhang, J., Wang, J., Tang, G., Wang, Y., 2016a. Characteristics, source apportionment and reactivity of ambient volatile organic compounds at Dinghu Mountain in Guangdong Province, China. Sci. Total Environ. 548–549, 347–359.
Wu, F.-k, Sun, J., Yu, Y., Tang, G.-q, Wang, Y.-S., 2016b. Variation characteristics and souces analysis of atmospheric volatile organic compounds in Changbai Mountain Station (in Chinese). Environ. Sci. 37.
Wu, W., Zhao, B., Wang, S., Hao, J., 2017. Ozone and secondary organic aerosol formation potential from anthropogenic volatile organic compounds emissions in China. J. Environ. Sci. 53, 224–237.
Xu, J., Zheng, L., Yan, Z., Huang, Y., Feng, C., Li, L., Ling, J., 2020. Effective extrapolation models for ecotoxicity of benzene, toluene, ethylbenzene, and xylene (BTEX). Chemosphere 240, 124906.
Xu, Z., Wang, T., Xue, L.K., Louie, P.K.K., Luk, C.W.Y., Gao, J., Wang, S.L., Chai, F.H., Wang, W.X., 2013. Evaluating the uncertainties of thermal catalytic conversion in measuring atmospheric nitrogen dioxide at four differently polluted sites in China. Atmos. Environ. 76, 221–226.
Xue, L.K., Wang, T., Guo, H., Blake, D.R., Tang, J., Zhang, X.C., Saunders, S.M., Wang, W. X., 2013. Sources and photochemistry of volatile organic compounds in the remote atmosphere of western China: results from the Mt. Waliguan Observatory. Atmos. Chem. Phys. 13, 8551–8567.
Yan, Y., Cabrera-Perez, D., Lin, J., Pozzer, A., Hu, L., Millet, D.B., Porter, W.C., Lelieveld, J., 2019. Global tropospheric effects of aromatic chemistry with the SAPRC-11 mechanism implemented in GEOS-Chem version 9-02. Geosci. Model Dev. 12, 111–130.
Yang, M., Wang, Y., Chen, J., Li, H., Li, Y., 2016. Aromatic hydrocarbons and halocarbons at a mountaintop in Southern China. Aerosol Air Qual. Res 16, 478–491.
Zeng, P., Guo, H., Cheng, H., Wang, Z., Zeng, L., Lyu, X., Zhan, L., Yang, Z., 2019. Aromatic hydrocarbons in urban and suburban atmospheres in central China: spatiotemporal patterns, source implications, and health risk assessment. Atmosphere 10, 565.
Zhang, J., Sun, Y., Wu, F., Sun, J., Wang, Y., 2014. The characteristics, seasonal variation and source apportionment of VOCs at Gongga Mountain, China. Atmos. Environ. 88, 297–305.
Zhao, R., Dou, X., Zhang, N., Zhao, X., Yang, W., Han, B., Yu, H., Azzi, M., Wang, Y., Bai, Z., 2020. The characteristics of inorganic gases and volatile organic compounds at a remote site in the Tibetan Plateau. Atmos. Res. 234, 104740.
Zhou, X., Beine, H.J., Honrath, R.E., Fuentes, J.D., Simpson, W., Shepson, P.B., Bottenheim, J.W., 2001. Snowpack photochemical production of HONO: a major source of OH in the Arctic boundary layer in springtime. Geophys. Res. Lett. 28, 4087–4090.